Slow earthquake in Afghanistan detected by InSAR

M. Furuya,[1] and S. P. Satyabala[2]

M. Furuya, Department of Natural History Sciences, Hokkaido University, N10W8, Kita, Sapporo, 060-0810, JAPAN. (furuya@mail.sci.hokudai.ac.jp)

S. P. Satyabala, National Geophysical Research Institute, Hyderabad, INDIA. (satyabala1978@yahoo.com)

[1]Department of Natural History Sciences,
Hokkaido University, Sapporo, Japan

[2]National Geophysical Research Institute,
Hyderabad, India.

The Chaman fault system forms a prominent ∼900-km-long left-lateral transform plate boundary between the Indian and Eurasian plates in Afghanistan and Pakistan. Here we show satellite radar interferometry data that revealed an afterslip (or slow earthquake) signal following an earthquake of magnitude 5.0. This slow slip episode lasted for more than a year, and accompanied a widespread creep signal that occurred at least ∼50 km along the fault. We detected no surface slip before the earthquake during the 1.5 years sampled by our data. This finding of long-lasting widespread afterslip demonstrates that the plate motion along the Chaman Fault is accommodated by slow slip episodes following moderate earthquakes, and suggests that a potential for magnitude 7-class earthquakes was significantly reduced. The duration and moment release of the detected afterslip do not fit the recently proposed scaling law for slow earthquakes.

1. Introduction

Crustal deformation measurements around plate boundaries by modern geodetic techniques have important implications for crustal rheology, fault mechanics, and seismic hazard assessment [*Sagiya*, 1999; *Bürgmann et al.,* 2000; *Fialko*, 2006]. Over the past decade, they revealed a variety of slow fault movements undetectable by seismometers not only in transform fault zones [*Linde et al.*, 1996] but also in subduction zones [*Kawasaki et al.*, 1995; *Heki et al.*, 1997; *Dragert et al.*, 2001; *Lowry et al.*, 2001; *Ozawa et al.*, 2002]. Following *Ide et al.* [2007], we call all these events slow earthquakes. Although slow movement (creep) has been known for decades in the San Andreas transform fault system, they have been regarded as exceptional because no similar phenomena have been reported in other continental strike slip faults [*Scholtz*, 1998; *Fialko et al.*, 2005].

While the relative slip velocity at the Chaman Fault, a major strike-slip fault in southwest Asia (Figure 1), has been geologically estimated to be 2–4 cm/yr [*DeMets et al.*, 1991; *Lawrence et al.*, 1992], historical records show an absence of large earthquakes at a 300–400 km segment of the Chaman Fault, suggesting that this segment of the fault is either locked or slipping aseismically [*Ambraseys and Bilham*, 2003]. Since modern ground-based geodetic measurements are infeasible now around this area, we employed space-borne Interferometric Synthetic Aperture Radar (InSAR) technique, using Envisat ASAR acquired by European Space Agency (Table S1), and detected postseismic deformation signal associated with the moment-magnitude (Mw) 5.0 earthquake on 21 October 2005 (Harvard CMT project).

2. Data Analysis and Results

Seven observed interferograms in Figure 1 are enlargements of the spatio-temporal evolution of the radar line-of-sight (LOS) changes. In order to reduce atmospheric artefact, each interferogram was generated by averaging two interferograms derived from two pre-earthquake images and one post-earthquake image acquired on (a) 17 days, (b) 52 days, (c) 122 days, (d) 192 days, (e) 332 days, (f) 367 days, (g) 543 days after the earthquake (Table S1). The signal pattern is consistent with left-lateral strike slip mechanism of the earthquake. Also, there are steps in the LOS changes across the fault and coherence losses around the epicenter (Figure S2), suggesting that the fault slip breached the surface at least within 17 days after the M5.0 earthquake; otherwise, they will change smoothly around the epicenter. Furthermore, not only the signal amplitude but also the spatial extent of deforming area clearly gets larger over time, thus demonstrating significant post-seismic deformation. The exact spatial extent and duration of surface deformation cannot be constrained because atmospheric effects are not completely corrected for. However, the clipped-out areas in Figure 1 should not seriously suffer from those noises, because as the spatial scale gets smaller, atmospheric signature becomes smaller in general [*Hanssen*, 2001]. Moreover, in full-scene interferograms, the jumps in the LOS changes show up more clearly over time, and do not localize around the epicenter but expand over at least 50 km along the fault even a year after the M5 event (Figure S1). To our knowledge, year-long postseismic deformation from a M5 earthquake has never been reported. The spatio-temporal coverage of the postseismic deformation in Figure 1 is thus unexpectedly long for M5.0 determined by seismic observation.

Three processes, visco-elasticity [*Pollitz et al.*, 2001; *Gourmelen and Amelung*, 2005], poro-elasticity [*Jónsson et al.*, 2003], and afterslip [*Heki et al.*, 1997; *Marone et al.*, 1991; *Freed*, 2007], are now widely known as the mechanisms for postseismic deformation [*Feigl and Thatcher*, 2006]. Since the earthquake we now encounter is M5 and its hypocenter is as shallow as ∼3 km as discussed below, and even the stress changes due to the 2004 M6 Parkfield event are shown to be too small to generate visco-elastic relaxation [*Freed*, 2007], it is unlikely for viscous relaxation from lower crust to upper mantle revealed on the surface. If poro-elasticity were significant, the spatial pattern of the postseismic deformation should be in inverse sense to the coseismic one, which is not the case in Figure 1, and suggests that poro-elastic processes were not playing a measurable role. This observation implies that afterslip is dominant, and model the observed postseismic deformation to infer the fault slip distribution, using dislocation Green function in an elastic, isotropic and homogeneous half space [*Okada*, 1992].

Figure 2 shows cumulative slip distribution of the optimum fault source model at each epoch. The maximum slip amplitude was initially about 6 cm at a depth of 2-3 km (Figure 2a). Whereas the afterslip propagated upward in the two cases in California, the 1987 Superstition Hills (Mw 6.6) and the 2004 Parkfield (Mw 6.0) events [*Bilham*, 1989; *Freed*, 2007], Figure 2 demonstrates that the afterslip area expanded downward over time, which is rather similar to the deep afterslip following the 1992 Landers [*Fialko*, 2004; *Perfettini and Avouac*, 2007] and the 1999 Izmit earthquake [*Bürgmann et al.*, 2002]. The estimated fault model allows us to compute cumulative moment released by each epoch (Figure 3). The moment magnitude released after the M5 event is estimated to be 5.5, significantly larger than the coseismic one. Logarithmic changes have been observed in a variety of tectonic settings [*Heki et al.*, 1997; *Marone et al.*, 1991], and it seems to fit reasonably well to this strike-slip earthquake as well, despite the orders-of-magnitude difference in the released moment.

To see if there was any steady creep motion before the earthquake, we generated three groups of stacked interferograms with different mean temporal coverage, each of which was generated by stacking three independent interferograms (Figure 4 and Table S2); no data after 21 Oct 2005 were used. If creep motion took place steadily with a constant rate, the deformation signal would be proportional to the temporal coverage. While we could identify such signals in the northwest near Qalat, that is presumably ground subsidence due to water pumping, the observed size of the phase jumps across the fault does not increase proportionally with time (Figure 4; see also Figure S6). We thus conclude that steady creep on the surface does not exist, at least, along the analyzed period and area.

3. Discussion

Of the seven data acquisitions after the earthquake, six allowed us to generate three independent postseismic interferograms (Table S2 and Figure S7). What should be noted is that the jumps across the fault in the radar LOS changes do not reveal any lobes around the epicenter but rather spread over a wide area along the fault. The LOS changes across the fault are observed not only around the epicenter but also, at least $\sim$50 kilometers-long portion along the fault, demonstrating that slip occurred over a broad area after the M5 earthquake. The slipped area in Figure 2 is therefore significantly under-estimated, suggesting that the total moment release would be much larger. Nevertheless, if considered as a single event with a duration of ∼1 year, the observed deformation does not fit the recently proposed scaling-law for slow earthquake, in which total moment is predicted to be $\sim 10^{19-20}$ Nm [*Ide et al.*, 2007]. The smaller moment release despite ∼1 year duration may be due to a strike-slip environment. Since the brittle-ductile transition depth is shallower than that in cold subduction zones [*Scholtz*, 1998], the depth extent of the fault would be at most 15 km. Unless the fault length extends hundreds of kilometers or more, it is unlikely for the total moment to reach $\sim 10^{19-20}$ Nm.

The previously estimated relative plate boundary velocity 2-4 cm/yr suggests that M $>$ 7 events could occur with $<$ 200 years intervals [*Ambraseys and Bilham*, 2003] or M $>$ 5 earthquakes with $<$ 2 years intervals. The earthquake catalogues tell us, however, that the 2005 M5 event was the second largest earthquake over the past three decades in this area (2 degree × 2 degree), and that the largest one was the 1992 M5.5 event $>$ 100 km to the south (USGS catalogue). More than 10 earthquakes with M $>$ 5 have been missing in the recent three decades. As we argued, however, the M5 earthquake appears to have triggered a widespread afterslip which lasted for more than a year at an average rate of ∼0.8 cm/yr along ∼50 km long portion of the fault (Figure S8). If the depth extent of the widespread afterslip is supposed to be 10 km, the moment release could reach as much as 3×10^{17} Nm, which is equivalent to about eight Mw 5.0 earthquakes. We can speculate that the 1992 M5.5 event generated similar postseismic deformation. Consequently, these M5-class events and their significant afterslip would be enough to account for the moment deficit, and should have significantly reduced the potential of M7 events.

Why did such a significant afterslip follow this small (M5) earthquake? Afterslip processes have been successfully interpreted within a framework of Dieterich-Ruina rate-and-state dependent friction (RSF) law [*Dieterich*, 1979; *Ruina*, 1983; *Scholtz*, 1998]. Our speculation is that, unlike a simplified layered friction rate parameter $(A - B)$ structure [*Scholtz*, 1998], velocity-weakening zones $(A - B < 0)$ are heterogeneously distributed in a spotty fashion over some depth interval, while velocity-strengthening zones $(A - B > 0)$ are widely distributed on the fault interface. We think that the M5 earthquake nucleated in a region congested with negative $A - B$ patches, although our fault source inversion cannot resolve such fine structure. The local lithology is quaternary sediment and tertiary flysch [*Lawrence et al.*, 1992], which are presumably unconsolidated and will make $A - B$ more positive [*Scholtz*, 1998; *Marone et al.*, 1991]. Recent simulation study successfully illustrated an evolution of afterslip and aftershocks on a fault surface with heterogeneously distributed negative $A - B$ patches over a positive $A - B$ background [*Liu and Rice*, 2005; *Kato*, 2007].

Our InSAR data implies that plate motion around the Chaman Fault is accommodated by infrequent moderate earthquakes accompanied by significant afterslip, and that, instead of great earthquakes as large as M7, numerous small earthquakes undetectable by global seismic network are taking place which probably accompany Å gsilent earthquakes Å h at depth [*Rubin et al.*, 1999]. While many slow earthquakes have been reported in subduction zones, the present finding of a long-lasting afterslip at another matured strike slip fault demonstrates that the San Andreas Fault is no longer an exception.

Acknowledgments. We thank K. Feigl and I. Johanson for critical reviews. We also thank R. Bilham, N. Kato, M. Nakatani and K. Heki for discussion. Original Envisat data are copyright of European Space Agency. This work was mostly done while MF was at Univ. of Tokyo, and was supported from the 21st Century COE program at Univ. of Tokyo, "Multi-Sphere Earth System Evolution and Variation Predictability", and the Grant-in-Aid for Scientific Research, Japan Society for Promotion of Science (19340123). This work was initiated when both authors were CIRES visiting fellows at University of Colorado at Boulder.

References

Ambraseys, N., and R. Bilham (2003), Earthquakes in Afghanistan, *Seismo. Res. Lett.*, *74*, 107–123.

Bilham, R. (1989), Surface slip subsequent to the 24 November 1987 Superstition Hills, California, earthquake monitored by digital creepmeters, *Bull. Seismo. Soc. America, 79*, 424–450.

Bürgmann, R., Schmidt, D., Nadeau, R. M., d'Alessio, M., Fielding, E., Manaker, D., McEvilly, T. V., and M. H. Murray (2000), Earthquake potential along the northern Hayward fault, California, *Science*, *289*, doi: 10.1126/science.289.5482.1178.

Bürgmann, R., Ergintav, S., Segall, P., Hearn, E. H., McClusky, S., Reilinger, R. E., Woith, H., and J. Zschau (2002), Time-space variable afterslip on and deep below the Izmit earthquake rupture, *Bull. Seismo. Soc. America, 92*, 126–137.

DeMets, C., Gordon, R. G., Argus, D. F., and S. Stein (1990), Current plate motions, *Geophys, J. Int.*, *101*, 425–478.

Dieterich, J. H. (1979), Modelling of rock friction: 1 Experimental results and constitutive equations, *J. Geophys. Res., 84*, 2161–2168.

Dragert, H., Wang, K. and T. S. James (2001), A silent slip event on the Cascadia subduction interface, *Science*, *292*, 1525–1528.

Fialko, Y. (2004), Evidence of fluid-filled upper crust from observations of postseismic deformation due to the 1992 Mw 7.3 Landers earthquake, *J. Geophys. Res., 109*, doi:10.1029/2004JB002985.

Fialko, Y., Sandwell, D., Simons, M. and P. Rosen (2005), Three-dimensional deformation caused by the Bam, Iran, earthquake and the origin of shallow slip deficit, *Nature*, *435*, doi:10.1038/nature03425.

Fialko, Y (2006), Interseismic strain accumulation and the earthquake potential on the southern San Andreas fault system, *Nature*, *441*, doi:10.1038/nature04797.

Feigl, K. L. and W. Thatcher (2006), Geodetic observations of post-seismic transients in the context of the earthquake deformation cycle, *C. R. Geosci.*, *338*, doi:10.1016/j.crte.2006.06.006

Freed, A. M. (2007), Afterslip (and only afterslip) following the 2004 Parkfield, California, earthquake, *Geophys. Res. Lett., 34*, doi:10.1029/2006GL029155.

Gourmelen, N. and F. Amelung (2005), Postseismic Mantle Relaxation in the Central Nevada Seismic Belt, *Science*, *310*, doi:10.1126/science.1119798.

Hanssen, R. F. (2001), Radar interferometry -Data Interpretation and Error Analysis-, 308 pp., Kluwer Academic Publishers, Dordrecht.

Heki, K., Miyazaki, S. and H. Tsuji (1997), Silent fault slip following an interplate thrust earthquake at the Japan Trench, *Nature*, *386*, 595–597.

Ide, S., Beroza, G. C., Shelly, D. R. and T. Uchide (2007), A scaling law for slow earthquakes, *Nature*, *447*, doi:10.1038/nature05780.

Jónsson, S., Segall, P., Pedersen, R. and G. Bjórnsson (2003), Post-earthquake ground movements correlated to pore-pressure transients, *Nature*, *424*, 179–183.

Kato, N. (2007), Expansion of aftershock areas caused by propagating post-seismic sliding, *Geophys. J. Int., 168*, 797–808.

Kawasaki, I., Asai, Y., Tamura, Y., Sagiya, T., Mikami, N., Okada, Y., Sakata, M., and M. Kasahara (1995), The 1992 Sanriku-Oki, Japan, ultra-slow earthquake, *J. Phys. Earth, 43*, 105–116.

Lawrence, R. D., Hasan Khan, S. and T. Nakata (1992), Chaman Fault, Pakistan-Afghanistan. *Ann. Tectonicae*, *6*, 196–223.

Linde, A. T., Gladwin, M. T., Johnson, M. J. S., Gwyther, R. L., and R. G. Bilham (1996), A slow earthquake sequence on the San Andreas fault, *Nature*, *383*, 65–68.

Liu, Y. and J. R. Rice (2005), Aseismic slip transients emerge spontaneously in three-dimensional rate and state modeling of subduction earthquake sequences, *J. Geophys. Res., 110*, doi:10.1029/2004JB003424.

Lowry, A. R., Larson, K. M., Kostoglodov, V. and R. Bilham (2001), Transient fault slip in Guerrero, southern Mexico, *Geophys. Res. Lett., 28*(19), 3753–3756.

Marone, C. J., Scholtz, C. H. and R. Bilham (1991), On the Mechanics of Earthquake Afterslip, *J. Geophys. Res., 96*, 8441–8452.

Okada, Y. (1992), Internal deformation due to the shear and tensile faults in a half-space, *Bull. Seismo. Soc. America, 82*, 1018–1042.

Ozawa, S., Murakami, M., Kaidzu, M., Tada, T., Sagiya, T., Hatanaka, Y., Yarai, H. and T. Nishimura (2002), Detection and monitoring of ongoing aseismic slip in the Tokai region, central Japan, *Science*, *298*, doi: 10.1126/science.1076780.

Perfettini, H. and J.-P. Avouac (2007), Modeling afterslip and aftershocks following the 1992 Landers earthquake, *J. Geophys. Res., 112*, doi:10.1029/2006JB004309.

Pollitz, F., Wicks, C. and W, Thatcher (2001), Mantle Flow Beneath a Continental Strike-Slip Fault: Postseismic Deformation After the 1999 Hector Mine Earthquake, *Science*, *293*, doi:10.1126/science.1061361.

Rubin, A. M., Gillard, D., and J. L. Got (1999), Streaks of microearthquakes along the creeping faults, *Nature*, *400*, 635–641.

Ruina, A. L. (1983), Slip instability and state variable friction laws, *J. Geophys. Res., 88*, 10359–10370.

Sagiya, T (1999), Interplate coupling in the Tokai district, Central Japan, deduced from continuous GPS data, *Geophys. Res. Lett., 26*(15), 2315–2318.

Scholtz, C. H. (1998), Earthquakes and friction laws, *Nature*, *391*, 37–42.

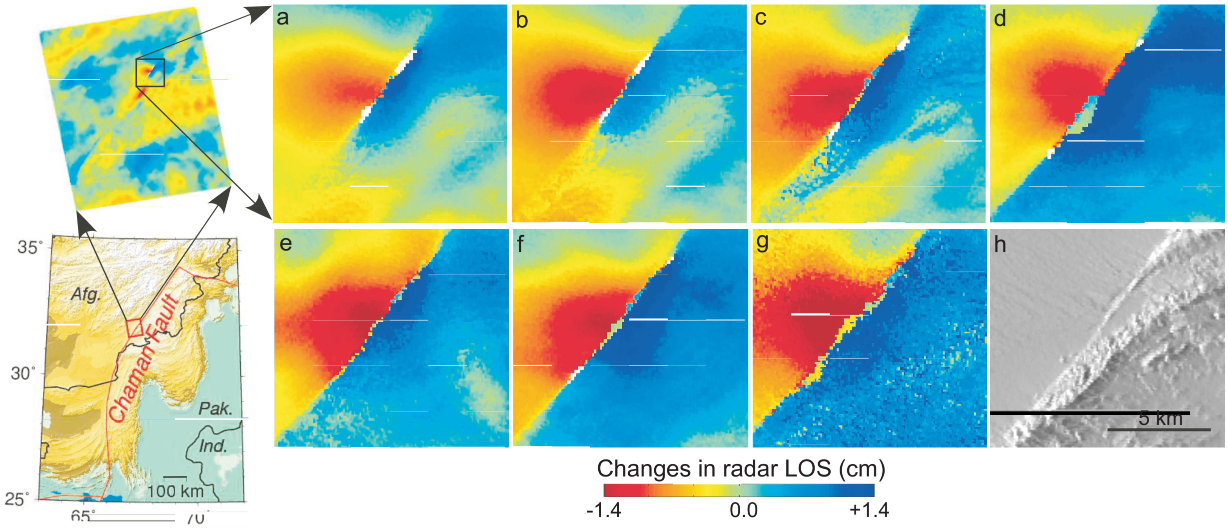

Figure 1. (Lower Left) Location map of the Chaman Fault (red line) and the analyzed full scene (red rectangle). Black solid lines are nations' boundary, and Afg, Pak, and Ind stand for Afghanistan, Pakistan, and India, respectively. (Upper Left) Full-scene InSAR data: see Figure S1 for all seven pairs. (Right) Expanded views of InSAR data (a-g) around the epicenter as a function of time after the earthquake: (a) 17 days, (b) 52 days, (c) 122 days, (d) 192 days, (e) 332 days, (f) 367 days, (g) 543 days. Shaded relief map in the same area is shown in (h). Positive (negative) change represents increase (decrease) in radar LOS. A coherence map for Figure 1a is shown in Figure S2. Details of interferometric pairs are shown in Table S1.

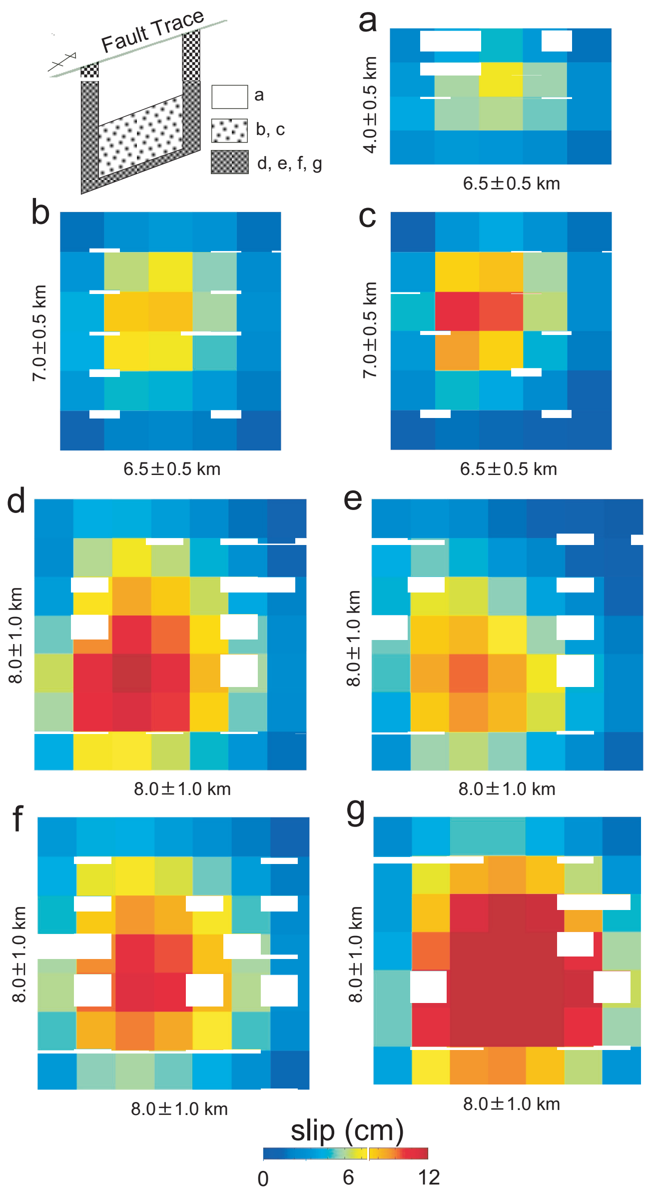

Figure 2. Each panel represents fault size with its uncertainty estimate and estimated slip distribution accumulated by (a) 8-Nov-2005, (b) 13-Dec-2005, (c) 21-Feb-2006, (d) 2-May-2006, (e) 19-Sep-2006, (f) 24-Oct-2006, and (g) 17-Apr-2007. Upper left panel shows the relative position of each fault model. The methods of error analyses are shown in auxiliary materials, Figures S3, S4 and S5.

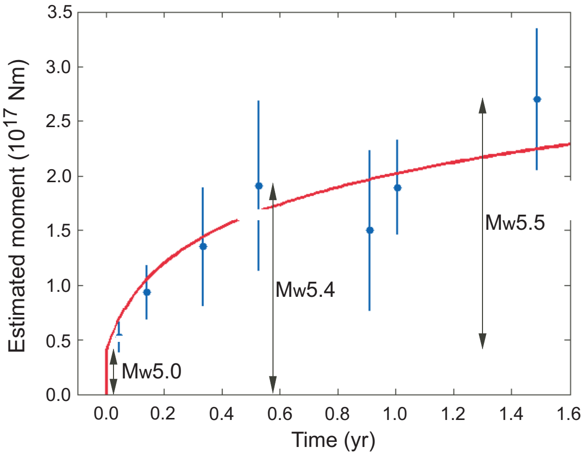

Figure 3. Temporal changes in the released moment (blue dots) estimated from the fault source models in Figure 2. Error bars represent 95 % confidence interval, which are estimated by the method described in auxiliary materials, Figures S3, S4 and S5. The post-seismic curve (red) is a logarithmic function whose temporal dependence is $\ln(pt+1)$ [*Marone et al.*, 1991], where p is optimized to be 3.6 yr^{-1}. Mw stands for moment magnitude.

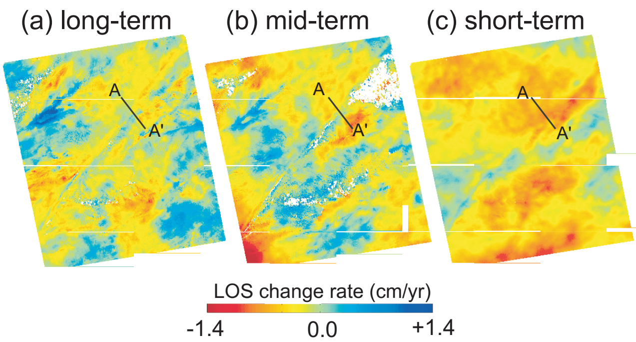

Figure 4. Three groups of pre-earthquake stacked interferograms; no data after 21 October 2005 are used. Three independent interferograms are stacked to generate each result (Table S2), but the average temporal separation is different in each stacked interferogram. In the actual stacking process, we have re-scaled the temporal separation in order to match it up with the average separation in Figure 4a. LOS changes of each interferogram along the profile A-A' are shown in Figure S6; A-A' crosses the epicenter of the M5 event.